Electromagnetic Spin–Field Dynamics

A material response model and new astrophysical tests

Research revision · 27 November 2026

Christopher Grenke's ESFD program began with a spinning top. As the top gained or lost stability, did its rotation change the alignment of its microscopic spins in a way a magnetic measurement could detect? This revision brings that question down to two independently varied quantities, an applied magnetic field and an angular speed. It then tests what two astronomical branches actually predict from the available observations.

The new material prediction

If a specimen's magnetic moment and spin angular momentum follow one equilibrated degree of freedom, a small change in rotation is equivalent to a signed shift in applied magnetic field. One measurement fixes the conversion between the two. It must then predict the shift at a second field and rotation rate. The simplest quartic version also fixes a fifth-order coefficient from two lower-order measurements. Both predictions can fail.

What the data changed

Question	Result in this revision
Does the ESFD curve predict outer speeds?	Across 21 held-out NGC 2403 radii, a flat extrapolation had a 6.64 km/s error and the anchored cored law had a 9.80 km/s error. The latter had a modest median advantage in two larger samples.
Does a magnetar stay on one side of the boundary?	One recovered spin-down range for 1E 1048.1−5937 spans index values of 0.345 to 1.260. A separate star supplies a test using an X-ray spectral feature.
Must an outward-moving model star return?	The archived logarithmic force confines every finite-energy orbit. An explicit outer flux that compensates at large radius permits escape for some of the same launch states.

The calculation uses the 123-page master, the posted Pattern Nexus edition, archived study inputs, the ESFD chats and 33 additional Word sources identified by file hash. New work and its assumptions appear on the following pages. The full master edition includes the earlier paper after this revision.

Pattern Nexus research edition · Published research tools

The recovered drafts define different fields

The 59-page June 3 manuscript and the 22-page *Proof* were already in the supplied packet. A separate ZIP and five adjacent Word files supply 34 distinct Word files in total. One is byte-identical to the June 3 manuscript. The other 33 are additional file versions. All 17 drafts named in the June consolidation can now be traced to files. Three other recalled inputs remain unnamed.

Source	Field definition or role in that source
4.1, §§3.1–3.3 · June 3, §3.3	Both use $X = S_{\mu\nu}S^{\mu\nu}$ and $V = \lambda(X - \Phi_0^2)^2/4$. Draft 4.1 prints $\Phi = \lambda^{-1/2}\sqrt{X}$. June 3 prints $\Phi = \sqrt{X}$. Their printed amplitude scales differ.
21, §§3.2–3.3	The clock proposal uses a contraction of spin with the electromagnetic field, $\Phi = \kappa\, S_{\mu\nu}F^{\mu\nu}$. A later expression introduces a charge normalization. At fixed spin this contraction reverses when the field reverses.
41, first synthesis §§1.3, 3.2–3.3 · 4.5, §3.2	The composite choice $\Phi = \kappa^2 X$ weights the Maxwell term by $\exp(-\xi\Phi)$. X is even under reversal of spin and independent of F at fixed spin. The first synthesis treats the scalar kinetic term as optional.
Spin-Entropy Field Dynamics · November master, §9	The recovered manifesto sets out the physical motivation. The quantitative current and effective-density equations used here are traced to the consolidation record and the November reconstruction.

A correction to the clock example

Draft 21 §3.2.1 inserts charge density, radius, angular speed and field into $\Pi = \rho_q R^2 \Omega B$. Its laboratory factors, multiplied by the stated 10^{-36}, give 2.09×10^{-31}. Its neutron-star powers give 10^{-9}, or 6.28×10^{-9} with the stated angular rate. The printed values are 10^{-9} for the laboratory and approximately one for the star. The original clock-rate estimates cannot be inferred from those substitutions.

In SI, Π has units of pressure. Multiplication by the draft's area-valued κ gives a force. One possible repair is $\Phi = \Pi/P_*$, with a pressure scale P_* calibrated independently. A clock test would constrain ξ/P_* and must identify which charge co-rotates. The arithmetic above supplies no measured clock offset.

Primary evidence in the companion archive · recovered-sources/source-manifest.csv and research-history.md. The 96-page Word metadata for 41 identifies a saved consolidation conversation. Its identity as the recalled standalone long master remains open.

From intrinsic spin to a rotating specimen

Start with the June 3 action, with direct interaction $\alpha S_{\mu\nu} F^{\mu\nu}$ and saturation energy $\lambda(X - \Phi_0^2)^2/4$. Bulk angular speed does not specify the spin tensor. To close that gap for a single material, consider a uniform specimen at fixed temperature with a reversible axial spin polarization p. Choose a rest frame and aligned axes. Take $S_{0i} = 0$ and $S_{ij} = S_* \varepsilon_{ij3} p$, so that $X = 2S_*^2 p^2$ in this coherent approximation. Spin fluctuations beyond this mean-field projection require extra material parameters.

Energy at prescribed field and rotation

$$f(p) = a\,p^2/2 + b\,p^4/4 - g\,p\,B - \ell\,p\,\Omega$$

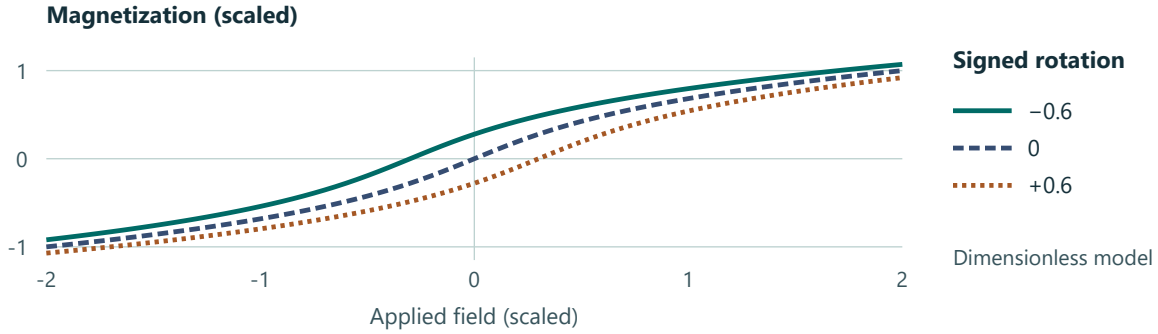
Here B is the calibrated axial field drive conjugate to magnetization, in tesla, with a consistent internal-field or demagnetization correction. Ω is the signed angular speed in rad/s. The dimensionless p carries magnetization $M = gp$ and spin angular-momentum density $j = \ell p$. Thus a and b have units J/m^3, g has units A/m, and ℓ has units $J\,s/m^3$. The two drive terms are energy densities. The spin part of the rotational work is $-\Omega j$. These are effective material coefficients.

Expanding the source potential with this projection gives $b = 4\lambda S_*^4$ and $a = a_{mat} - 2\lambda S_*^2 \Phi_0^2$ in a common unit convention. The additional material stiffness a_{mat} is an assumption. The direct spin–field term sets a contribution to g after field normalization and coarse graining. Neither g nor ℓ is determined by measuring the rigid-body angular speed alone.

What follows for the positive-stiffness branch

$$h = gB + \ell\Omega,\quad a\,p + b\,p^3 = h,\quad K = a + 3b\,p^2$$

For $a > 0$ and $b > 0$, K is positive and the stationary point is unique. At small drive $f_{min} = -h^2/(2a) + b\,h^4/(4a^4) + \ldots$. Its mixed energy term is $-(g\ell/a)B\Omega$. This supplies one material interpretation of a signed $B\Omega$ product. The curvature stays positive as the product changes. A universal collapse threshold needs additional physics. The model applies locally in the reversible range before higher powers, domains or hysteresis become important.



June 3, §§3.2–3.4 · recovered 4.1, §3 · November master, §§3–4. Background on magnetization by rotation and the magnetic equation of state.

Two ways to test the material model

Field and rotation must give the same shift

> $M(B, \Omega) = M(B + \ell\Omega/g, 0)$ for $g \neq 0$

At a given operating point, the derivatives of (M, j) with respect to (B, Ω) are $K_{BB} = g^2/K$, $K_{B\Omega} = K_{\Omega B} = g\ell/K$ and $K_{\Omega\Omega} = \ell^2/K$. Consequently $K_{BB}K_{\Omega\Omega} - K_{B\Omega}{}^2 = 0$. The determinant tests whether one coordinate supplies both responses after background subtraction. Reciprocity alone gives equality of the cross derivatives. Two responsive coordinates with different magnetic-to-angular ratios give a positive determinant when both stiffnesses are positive.

Determine ℓ/g on one slow field sweep with signed rotation. Use it to predict an independently repeated field sweep at a second Ω. A field-dependent shift, outside calibrated uncertainty, rejects the one-coordinate model with constant couplings. A full determinant test also needs independent angular-momentum readout and subtraction of rigid-body inertia. Measure field gradients, apparatus torque and ordinary magnetomechanical effects on separate controls. Ordinary magnetization can satisfy this null too.

A fifth-order prediction from two fitted coefficients

> $M(B, 0) = c_1B + c_3B^3 + c_5B^5 + \dots$, $c_1c_5 - 3c_3{}^2 = 0$

Series inversion gives $c_1 = g^2/a$, $c_3 = -bg^4/a^4$ and $c_5 = 3b^2g^6/a^7$. These are Taylor coefficients, with the factorials absorbed. A sixth-order term in the energy changes c_5. An independent two-state spin response proportional to $\tanh(B/B_0)$ gives $c_1c_5/c_3{}^2 = 1.2$. The quartic branch gives 3. Fit the first and third coefficients on a reversible calibration range, freeze the fifth-order prediction and test it against independent symmetric-field sweeps. Report coefficient covariance and field-window sensitivity. Use the undivided residual when c_3 is near zero.

The companion code checks the derivatives by finite differences across four states, the Taylor relation by exact rational arithmetic, and the determinant on a two-mode control. Its 243 sweep rows are model outputs. With a free-electron gyromagnetic magnitude only as a scale reference, 1 Hz of mechanical rotation corresponds to 35.68 pT. A specimen requires its own signed coefficient.

Derivation in this revision · research/spin_response/response.py and response_checks.json. Free-electron scale from NIST CODATA.

The far field of the direct coupling

The *Proof* proposes that spin–field energy generates an effective gravitational metric. Its displayed interaction permits a narrower calculation immediately. Hold the background geometry flat, use ordinary Maxwell propagation outside a compact source, take the spin tensor as a stationary localized source, and consider a neutral probe. This fixes the spatial decay of the direct electromagnetic channel.

$$H^{\mu\nu} = F^{\mu\nu}/\mu_0 - \kappa S^{\mu\nu},\ j_{\mathrm{pol}}{}^{\nu} = \kappa\, \partial_{\mu} S^{\mu\nu}$$

The effective polarization current is conserved by antisymmetry. Its net electric charge is proportional to the surface integral of S^{i0} at infinity. That integral vanishes for localized spin. For a purely spatial, stationary spin distribution the leading nonzero external magnetic field can be a dipole. Its axial amplitude scales as r^{-3}.

Probe response at large r	Energy scaling	Force scaling
Permanent aligned moment in a dipole field	$-\mu B \propto r^{-3}$	Magnitude $\propto r^{-4}$, with orientation dependence
Linear induced moment with fixed polarizability	$-\alpha_m B^2/2 \propto r^{-6}$	Magnitude $\propto r^{-7}$, with material dependence
Universal Newtonian monopole target	$-GMm/r$	Magnitude GMm/r^2

A vanishing dipole gives still faster falloff for these channels. This restricts the proposal that the direct local coupling alone supplies ordinary gravity from an isolated neutral rotating body. Extended currents, a separate propagating field or a metric response change the assumptions and need their own source law. The June action's Einstein–Hilbert term already transmits a long-range gravitational response to total stress with an input G.

What a gravity completion must calculate

A separate gravity branch must specify which field carries the monopole, why its source follows total mass-energy, and how neutral probes of different materials respond. Galaxy kinematics constrain the slow-matter potential Ψ. Lensing constrains the combination $\Psi + \Phi$ of metric potentials. A single fitted acceleration profile cannot determine both. The compensated example on the next page supplies a source diagnostic while leaving the metric matching open.

Proof of the Electromagnetic Spin–Field Dynamics Theory, pp. 1–4 · June 3, §3.2 · November master, §§4 and 9. The falloff follows by differentiating the two probe energies above.

Will a displaced star return?

The saved simulator export has 271 radii. At 20.6 kpc its ESFD circular speed is 143.323 km/s. The export was in baryons-only mode, where the circular speed is 67.975 km/s. Its separate ESFD column reproduces the published force law. Preserving the orbital velocity while switching to baryons alone can release a star because the local baryonic escape speed is only 98.066 km/s.

Write $r_c = 4.179$ kpc and $V^4 = GM_b a_*$ for the archived synthetic disk. Its additional inward acceleration is $g_0 = V^2 r/(r^2 + r_c^2)$. Its logarithmic potential grows without bound. In the spin–entropy branch the effective density is a spatial divergence, $\rho_x = \nabla \cdot Q$, with the phenomenological normalization absorbed in Q. A local Euclidean spherical example that compensates at infinity is

$$g_t(r) = g_0(r)\, R_t^2/(r^2 + R_t^2),\ Q_r = g_t/(4\pi G),\ M_x(<r) = r^2 g_t/G.$$

For a regular center the extra enclosed mass tends to zero at both ends. Its derivative changes sign. The negative outer contribution is an effective density correction. Choosing a reach R_t is an assumption. The closed-space integral constraint alone fixes no transition radius.

For $a = r_c^2$ and $b = R_t^2$, the potential with zero at infinity is $\Phi_t = V^2 b \ln[(r^2 + a)/(r^2 + b)]/[2(b - a)]$ for $b \neq a$. At 40 kpc reach the effective density crosses zero at 40.84 kpc. This radius identifies where outer matter-tracer or lensing observations could start to distinguish the source shapes, once their coupling to light is specified.

Stationary potential	Escape speed at launch	Outer turn after +12 km/s	Outer turn after +180 km/s
Baryons only	98.1 km/s	Escapes	Escapes
Reach 40 kpc	187.4 km/s	27.3 kpc	Escapes
Reach 80 kpc	234.8 km/s	22.8 kpc	258.0 kpc
Reach 160 kpc	277.9 km/s	22.1 kpc	91.8 kpc
Original logarithm	Unbounded	21.9 kpc	80.3 kpc

Every row starts at 20.6 kpc with tangential speed 143.323 km/s and the indicated outward speed. The 12 km/s value matches one simulator nudge. The 180 km/s value illustrates reach sensitivity. The turning radii solve the energy equation with angular momentum fixed in each potential. Large excursions extrapolate beyond the exported disk. A past screenshot alone cannot recover a particular trajectory.

Archive · Research/3D_Galaxy/physics.py and model.js. Supplied simulator export and numerical checks · research/spin_entropy/.

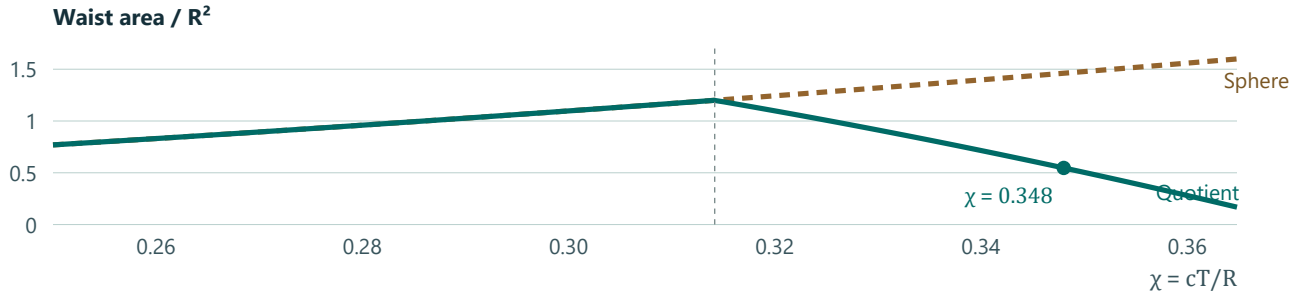
How much of the causal diamond is geometry?

The stored three-panel figure marks $\chi = cT/R = 0.348$, with endpoints separated by 2T. Its comparison is between the round 3-sphere and its Poincaré dodecahedral quotient at the same curvature radius R. The figure supplied the coordinate. The following area is calculated directly from the face geometry.

The centered spherical cell has twelve nearest faces at angular distance $f = \pi/10$. On a geodesic sphere of radius $R\chi$, each face excludes the directions in a cap whose limiting direction cosine is $u = \tan(f)/\tan(\chi)$. Up to the first edge at $\chi \approx 0.364864$ the caps are disjoint. Each covers a fraction $(1 - u)/2$ of the angular sphere. Thus, in the interval $f < \chi < \chi_{edge}$,

$$A_{quotient}/A_{sphere} = 1 - 6(1 - u),\ A_{sphere}/R^2 = 4\pi \sin^2\chi.$$

At 0.348 the two areas divided by R^2 are 0.546665 and 1.461388. The quotient area is **62.593% smaller**. Testing 60,000 nearly uniform directions independently gives a surviving fraction of 0.373767 versus the analytic 0.374073. This reproduces the earlier chat's rounded 62.6% with the spin current set to zero. It is a geometric baseline for the model.



A wave observable with a separate source test

On this static quotient the first two nonconstant scalar harmonics have k = 12 and 20. Write $\omega_k^2 = \omega_0^2 + c_s^2 k(k+2)/R^2$ for the linear entropy mode. The shortest light loop takes $\tau = \pi R/(5c)$. Consequently

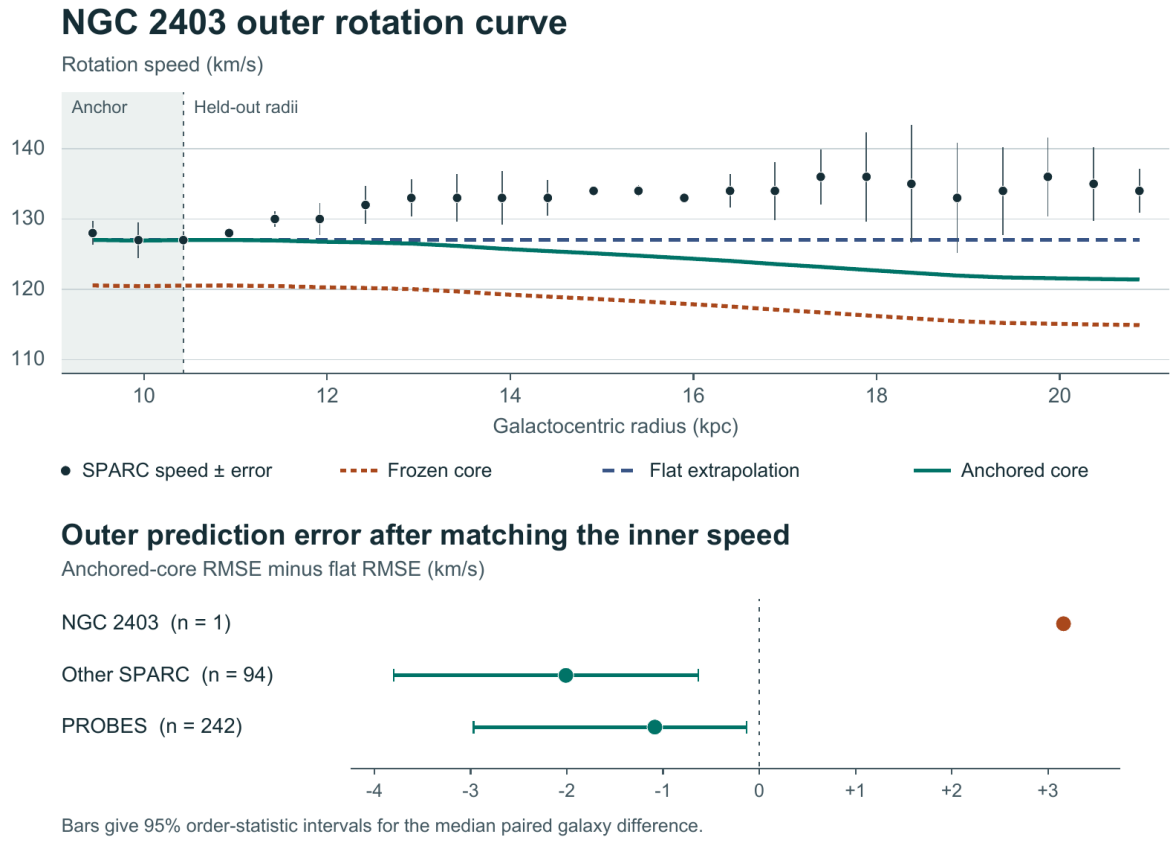
$$\tau \sqrt{(\omega_{20}^2 - \omega_{12}^2)} = (\pi/5)\sqrt{272} \cdot (c_s/c) = 10.3625 \cdot (c_s/c).$$

The curvature radius and the common frequency offset cancel. In the archived linearized field equation the imposed drive is proportional to $-\beta_s \nabla_\mu J_s^\mu$. Reversing a prescribed current reverses the driven perturbation at identical initial conditions after subtracting the undriven solution. Its sign tests a source coupling. The separate identity $\int \nabla_i (s J_s^i)\, dV = 0$ holds on a closed spatial slice. It constrains total effective density. Neither result establishes the topology of our universe.

Original Poincaré-space model · Scalar modes, Table 1 · Injectivity radius · Published figure discussion.

NGC 2403 and the shape of the outer curve

The SPARC table gives 134.00 ± 3.12 km/s at 20.87 kpc. Reserve all 21 radii beyond 10.435 kpc. The last three distinct inner radii have speeds of 128, 127 and 127 km/s. Anchor each model to their median before extrapolating its shape. This gives a flat extrapolation and two shaped predictions with the same information about inner speed.



The archived frozen core has an outer root-mean-square error of 15.98 km/s. Anchoring lowers it to 9.80 km/s. The anchored baryonic shape gives 14.65 km/s and the flat extrapolation gives 6.64 km/s. A separate two-parameter slow-approach model fitted to the inner data in the prior master reaches 4.90 km/s. The figure shows the published speed errors. The held-out scores are unweighted and the comparison is retrospective.

Across other eligible galaxies, the anchored core beats flat in 58/94 SPARC and 139/242 PROBES cases. The median paired differences in km/s are −2.01 [−3.80, −0.64] and −1.09 [−2.97, −0.13]. The 95% order-statistic intervals treat galaxies as independent within each selected sample. Shared survey systematics remain. The predictor uses baryonic inputs and an empirical acceleration. Independent field measurements would be needed to attribute a shape advantage to electromagnetic dynamics.

SPARC measurements · PROBES data, Stone et al. · read research/galaxy/README.md for eligibility, matched baselines and per-galaxy scores.

A magnetar can cross the timing boundary

The June manuscript uses $\chi = B\Omega/\Lambda$ with $\Lambda = 6.28 \times 10^{14}$ G rad/s. With an equatorial timing estimate $B = 3.2 \times 10^{19}\sqrt{(P\dot{P})}$ G and $\Omega = 2\pi/P$, its meaning is fixed algebraically.

> $\chi = \sqrt{(\tau_*/\tau_c)}$, $\tau_c = P/(2\dot{P})$, $\tau_* = 1{,}624.076$ years.

The catalog ratio ranks sources in exactly the same order as inverse characteristic age. Among 2,898 positive ATNF timing pairs, five of 22 anomalous X-ray pulsar tagged sources and four of 2,876 others pass $\chi \geq 1$. The ranking probability (AUC) is 0.936686 using either χ or inverse characteristic age. These are catalog classifications. Characteristic age is a timing proxy.

Using the separate McGill primary selection, five of 22 uncensored confirmed magnetars pass. Two more confirmed sources have upper limits already below one. The source lists six spin-down ranges beyond the alternate point estimates in the archived atlas. Their endpoints summarize changes over observing intervals. Each uses the primary period because that alternate row omits a period.

Star	Timing reference in the McGill table	Recalculated χ range
1E 1048.1–5937	gk04 · then dkg09	0.345–1.260 · then 0.445–0.891
1E 1547.0–5408	crj+08	1.078–1.250
PSR J1622–4950	lbb+12	0.471–0.678
SGR 1806–20	wkf+07	1.971–3.319
XTE J1810–197	ccr+07	0.282–0.439

One star, two different classifications

For 1E 1048.1–5937 the primary χ is 0.598. The broader published range in $\dot{P}$ spans 7.5×10^{-12} to 1.0×10^{-10} s/s. At the listed period this crosses one. The source associates no timestamp with these two extrema. A time series, contemporaneous activity records and monitored exposure would be needed to test whether crossings precede events.

McGill Magnetar Catalog · Original torque monitoring · ATNF catalog. See research/stars/ for every recovered range.

Testing the threshold with an independent field estimate

An X-ray line provides information beyond the period derivative. A quiescent XMM-Newton observation of 1E 2259+586 on 29 July 2014 measured a period of 6.979164(1) s. Pizzocaro and colleagues fitted a broad absorption feature in that same observation. The result below asks what the ESFD threshold would imply if the feature is a proton cyclotron fundamental.

> $B_{line}/(10^{14}\ G) = E_{line}(1 + z)/(0.63\ keV)$, $B_{\chi=1} = \Lambda P/(2\pi)$.

At the assumed redshift z = 0.25, the period sets $B_{\chi=1} = 6.976 \times 10^{14}$ G. A proton fundamental at that field would be observed at **3.516 keV**. The observed feature was fitted at much lower energy in both detector analyses.

Same observation	Fitted centroid	Conditional ESFD index
EPIC-pn	0.68 ± 0.07 keV	0.193 ± 0.020
EPIC-MOS	0.87 ± 0.02 keV	0.247 ± 0.006

The errors propagate the published centroid and period uncertainties at fixed redshift. The instrument-dependent difference illustrates a larger interpretive uncertainty. Line identity, continuum choice, redshift and the relation between local and large-scale field affect the result. Both estimates describe one target at one epoch.

A prospective event comparison

Specify the physical field in the index before scoring. Define the flare-energy threshold, monitoring window and treatment of non-detections before inspecting events. Estimate fields using pre-event observations independent of $\dot{P}$ and retain instrument and epoch information. Compare held-out stars with a timing-age model using the same exposure. A calibrated excess in the high-index group would support that field-specific prediction. A null limits its event-rate contrast at the sensitivity achieved. This test needs observing data beyond the recovered snapshot.

Pizzocaro et al., §§3–5 and Table 2 · XMM observation 0744800101 · research/stars/results.json contains the two instrument estimates and assumptions.

What remains open across the program

The final archived master register contains 75 branches. The companion research package preserves every original register row and adds revision entries to 13. The other rows retain the evidence assigned to them in that master. The requirements below identify measurements or calculations that could change the interpretation of particular branches.

Branch	What would move it forward
Rotation, material response and superconductors	Measure the signed M(B, Ω) shift on one calibrated specimen. Record temperature, magnetic history and the blank apparatus response. Use frozen coefficients for held-out sweeps. The existing ring, disk, phase and downward-probe runs are simulations. A force on a separate probe needs an independent acceleration channel.
Gravity, inertia and galaxy fields	Supply a conserved stress or a matter metric, its normalization and couplings to neutral matter and light. Freeze the outer radial law and independently measure ordered field, gas density and their gradients where an outer speed prediction is tested. An inverse field profile calculated from those speeds reuses the target.
Compact objects, bursts and collapse	Use independent field measurements and event exposure. A collapse calculation needs an equation of state, stable and unstable solutions, and an identifiable signal. Timing thresholds alone cannot give a black-hole boundary.
Quantum coherence, collider and cosmology	Specify a detector observable and alternate-model prediction using common acceptance and uncertainties. The archived Bell, off-shell Higgs, lensing, cosmic topology and bounce discussions concern different underlying tests. A shared spin symbol does not fix their couplings.
Waves, solar activity and other tests	The standing-wave and material simulations establish behavior for specified sources. Time-domain solar or high-energy event tests need held-out epochs and exposure-aware null models. Raw files for some historical FDTD, GRMHD and rotor-clock claims remain unlocated.

The next measurement with the shortest path back to the original spinning-top question is a calibrated, reversible field-and-rotation response. It addresses the distinction between rigid-body motion and microscopic polarization before introducing a gravitational or astronomical coupling. For the galaxy branch, an independently measured field profile is the missing input with the most direct bearing on the proposed force.

Archived register · branch_register.csv in the prior November master package. This revision's full register and verification are in research/branch_register.csv and research/source_audit.json.

Sources and reproduction

Project record

The supplied 495,972,821-byte research ZIP has 638 members. All 637 catalogued files verified against their SHA-256 values. The catalog itself is the remaining member. The master PDF and NGC 2403 data ZIP match the retained Pattern Nexus upload byte-for-byte. The 3D galaxy page also carries the same numerical payload. The private recovery ledger records the accessible chat windows, original filenames and unresolved leads. File identity and page metadata alone do not authenticate scientific claims.

Run the calculations

Extract the companion research ZIP and run **python research/run_checks.py** with Python 3.9 or newer. The four research calculations use the Python standard library and read included inputs. The runner regenerates the numerical outputs in a temporary folder and compares them with the delivered tables. The individual methods and data names appear alongside each analysis. The optional source audit reads the original 496 MB ZIP to recheck the historical catalog and register.

Folder or file	What it contains
research/spin_response	Equilibrium response, exact expansion coefficients, reversal sweep, determinant tests and draft 21 arithmetic.
research/spin_entropy	The 271-row simulator export, compensated source profiles, orbital turning points, face-cap area calculation and mode spacing.
research/galaxy	Two frozen curve inputs, 19,152 radius rows across 376 galaxies, eligibility and paired prediction errors.
research/stars	Frozen timing inputs, row-level range audit, June example recalculations and the independent spectral comparison.
recovered-sources · research-history.md	Original recovered research files, hashes, chat and manuscript identification, and outstanding recovery leads.

Primary references for the relevant calculations accompany each chapter. The following releases identify the observing teams and the versions underlying the data selections. Historical expressions are attributed to their source drafts. The closure, compensated example and new comparisons are research extensions introduced here.

SPARC · PROBES · ATNF · McGill · XMM analysis · ESFD master and original tools.